AGU PUBLICATIONS

Global Biogeochemical Cycles

Supporting Information for

Transport of anthropogenic carbon from the Antarctic shelf to deep Southern Ocean triggers acidification

Shuang Zhang[1, 2, 3], Yingxu Wu[2]*, Wei-Jun Cai[4], Wenju Cai[5], Richard A. Feely[6], Zhaomin Wang[7], Toste Tanhua[8], Yanmin Wang[2,3], Chengyan Liu[5], Xichen Li[9], QinghuaYang[5], Minghu Ding[10], Zhongsheng Xu[11], Rodrigo Kerr[12], Yiming Luo[5], Xiao Cheng[5], Liqi Chen[1,2,3]*, Di Qi[2,7]*

[1]State Key Lab of Marine Environmental Science, Xiamen University, Xiamen, Fujian, China

[2]Polar and Marine Research Institute, Jimei University, Xiamen, Fujian, China

[3]The Third Institute of Oceanography (TIO), MNR, Xiamen 361005, China

[4]School of Marine Science and Policy, University of Delaware, Newark, Delaware 19716, USA

[5]Centre for Southern Hemisphere Oceans Research (CSHOR), CSIRO Oceans and Atmosphere, Hobart, Tasmania, Australia

[6]Pacific Marine Environmental Laboratory, National Oceanic and Atmospheric Administration, Seattle, WA 98115–6349, USA.

[7]Southern Marine Science and Engineering Guangdong Laboratory (Zhuhai), China

[8] GEOMAR Helmholtz Centre for Ocean Research Kiel, Kiel, Germany

[9]International Center for Climate and Environment Sciences, Institute of Atmospheric Physics, Chinese Academy of Sciences, Beijing 10029, China

[10]Chinese Academy of Meteorological Sciences, Beijing 100081, China

[11]Key Laboratory of Marine Ecosystem and Biogeochemistry, Second Institute of Oceanography, Ministry of Natural Resources (MNR), Hangzhou, China

[12]Laboratório de Estudos dos Oceanos e Clima, Instituto de Oceanografia, Universidade

Federal do Rio Grande (FURG), Av. Itália km 8, Rio Grande, 96203-900, RS, Brazil

*Corresponding authors:

Di Qi (qidi@jmu.edu.cn); Yingxu Wu (yingxu.wu@jmu.edu.cn); Liqi Chen (chenliqi@jmu.edu.cn)

Contents of this file:

Text S1 to S5

Figures S1 to S13

Tables S1 to S6

Text S1

Quality control of CHINARE 31st discrete DIC and TA. DIC was measured using a non-dispersive infrared CO_2 analyser (Apollo SciTech, USA), each seawater sample (0.5 mL) was acidified with phosphoric acid and the evolved CO_2 gas was extracted and carried by pure N_2 gas to an infrared CO_2 detector (Li-Cor 6262) for quantification. TA was measured using the open-cell Gran titration method (Apollo SciTech, USA), using 0.1 M hydrochloric acid and an open-cell titration system. Both measurements related to marine carbonate systems followed the "Guide to Best Practices for Ocean CO_2 Measurements" (Dickson et al., 2007). The data quality of DIC and TA is constrained by the mature analytical techniques, and for each DIC or TA sample, subsamples were sequentially analyzed 2 or 3 times until we obtained two replicates with a precision within 0.1%. Therefore, the precision of DIC and TA measurements are better than 0.1% (uncertainty of 2 μmol kg^{-1}) (Chen et al., 2015). DIC and TA were calibrated using certified reference material (CRM) supplied by A.G. Dickson, Scripps Institution of Oceanography (USA). All figures and analyses in this manuscript include synthetic data (GLODAP and CHINARE 2015 in Fig. S1), except for some special notes.

Text S2

Calculation of air-sea fluxes in the Antarctic coastal seas. In the Pan-Antarctic (>60°S) shelf regions, early spring and winter often act as weak sources of atmospheric CO_2 due to low biological activity, while it represents a strong carbon sink from mid-spring to late autumn (Gibson and Trull, 1999; Gray et al., 2018; Shadwick et al., 2021). Taking into account cooling and the biological production, it is assumed that the outgassing flux in early spring and winter is by a compensation in autumn and mid-spring (Arrigo and Van Dijken, 2007; Gibson and Trull, 1999; Shadwick et al., 2021), i.e., the annual net gas exchange flux at the air-sea interface can be approximately equivalent to four months of CO_2 uptake (~120 days, covering the austral summer from mid-November to mid-March) (Constable et al., 2014; DeJong and Dunbar, 2017; Roden et al., 2013). The area of sub-region was calculated using a geographic information system (GIS, ArcGIS Desktop10.7, https://www.esri.com/en-us/arcgis/products/arcgis-desktop/overview) based on the Margins and Catchments Segmentation number 45 (MARCAT #45) according to Laruelle et al. (2013, 2014), where the offshore boundary of the continental shelf is characterised by the shelf break, the depth of which is calculated using a high-resolution global bathymetric database (Laruelle et al., 2013; Laruelle et al., 2014). Due to the scarcity of the data in the SOCATv4 dataset (Pfeil et al., 2013) and floats data for this region, and an overestimation or underestimation of carbon outgassing from Southern Ocean upwelling was unclear (Gray et al., 2018; Laruelle et al., 2017; Long et al., 2021; McNeil et al., 2007; Prend et al., 2022; Roobaert et al., 2019; Wu et al., 2022). We collected and recalculated the air-sea CO_2 fluxes based on different datasets in the Antarctic coastal seas from 27 Antarctic research cruises (Table S5). By dividing the shelf into cold shelf regions with four sub-regions named cold shelf regions (Table S5) and non-cold shelf regions with another four sub-regions (Table S5). A mean annual air-sea flux for each region from each daily air-sea CO_2 flux and a four-month open water duration, was used to estimate sub-region air-sea CO_2 flux (Table S5). The mean annual flux density (mol C m^{-2} yr^{-1}) was calculated for each sub-region and then was extrapolated to the cold shelf regions, and the entire Pan-Antarctic (>60°S) shelf regions based on the surface areas (Fig. 3). Finally, we roughly assessed the mean air-sea CO_2 flux of the Pan-Antarctic shelf region (>60°S), which was updated to -30.9 ± 6.1 Tg C yr^{-1} during 1990 to 2020 (Fig. 3 and Table S5).

Text S3

ΔC* approach improvement and Optimum multiparametric (OMP) analysis. For ΔC* approach improvement, we have performed three views to improve its application in Pan-Antarctic regions. We used an OMP analysis to evaluate the disequilibrium correction (Sabine and Gruber, 2005) and the oxygen saturation correction.

Our OMP analysis was set with five input variables: potential temperature (θ), salinity (S), NO (= O_2 + 9.3 NO_3), PO (= O_2 + 170 PO_4), and SiO_4. A mass balance equation was written for each variable.

$$\sum_{i} x_{ij}\theta_i = \theta_j + R_{\theta j} \quad (1)$$

$$\sum_{i} x_{ij}S_i = S_j + RS_j \quad (2)$$

$$\sum_{i} x_{ij}NO_i = NO_j + RNO_j \quad (3)$$

$$\sum_{i} x_{ij}PO_i = PO_j + RPO_j \quad (4)$$

$$\sum_{i} x_{ij}(SiO_4)_i = (SiO_4)_j + RSiO_{4j} \quad (5)$$

$$\sum_{i} x_{ij} = 100\% + R \quad (6)$$

where xij is the fraction of WTi in sample j; θ_i, S_i, NO_i, PO_i, and SiO_{4i} are the values of θ, S, NO, PO, and SiO_4 of WT i given in Table S2; θ_j, S_j, NO_j, PO_j, and SiO_{4j} are the values of θ, S, NO, PO, and SiO_4 in sample j; and $R_{\theta j}$, R_{Sj}, R_{NOj}, R_{POj}, R_{SiO4j}, and $R_{\sum}$ are the residuals of the mass balance equations of θ, S, NO, PO, SiO_4, and mass conservation for sample j. The set of equations contains two additional constraints: the contributions from all sources must sum to 100% (equation (6)), and all contributions must be non-negative (i.e., $x_{ij} \geq 0\%$). The equation for each variable was normalised and weighted. The equations were normalized by subtracting the mean and dividing by the standard deviation (SD) of the WT values (Table S2) of each variable. The weights were set to 8, 4, 3, 2, and 1 for potential temperature, salinity, NO, PO, and SiO_4, respectively (Romera-Castillo et al., 2019). In addition, a weight of 100 was assigned to the volume equation to ensure that it was strictly conserved. The characteristics of the WTs in their respective source regions (Table S2) were taken from the literature (Pardo et al., 2014; Pardo et al., 2012). The results of the four water source fractions are shown in Fig. S4.

Fig. S3 describes the TA^0 used in previous studies in different open oceans (Pacific Ocean, Indian Ocean and Atlantic Ocean), but these results based on the data were mostly located north of 60°S, so we regress a new TA^0 based on the surface TA data in the south of 60°S (Eq. 6 in Methods).

ΔC_{diseq} and oxygen saturation based on OMP analysis. Previous ΔC_{diseq} were taken from

Sabine et al. (1999, Tables 2 and 3), which remained large uncertain in the Pan-Antarctic due to air-sea disequilibrium. We also corrected the oxygen saturation value calculated in HSSW for a mean undersaturation α =12%. The oxygen saturation correction is applied to the deep ocean using the mixing ratio of HSSW (k). The following formulation is used for oxygen utilization:

$$\Delta O_2 = \left(1 - \alpha k\right) O_2^{sat} - O_2^{m} \qquad (7)$$

ratio k is determined using a mixing model described by Lo Monaco et al. (2005) based on the optimum multiparametric (OMP) analysis.

Text S4

Uncertainties in C_{ant} estimation and export flux. For the TrOCA approach, using the error propagation technique associated with DIC, TA, O_2, potential temperature, and other parameters in Eq. 3 (Methods), Touratier et al. (2007) estimated an uncertainty of 5.94 μmol kg^{-1}. For the ΔC* approach, the uncertainty is of the order of 6.10 μmol kg^{-1} as evaluated by Lo Monaco et al. (2005) due to O_{sat}, TA^0, ΔC_{diseq} estimation. Taking Δ/Γ, CFC surface saturation, the empirical relationship for TA^0, and dissociation constants into account, the uncertainty of TTD approach for C_{ant} estimation was 6.00 μmol kg^{-1} (Waugh et al., 2006). In addition, the uncertainty in the carbon export fluxes were evaluated by Monte Carlo method, where the propagated errors in C_{ant} estimations and ventilation rates that based on the observed CFC saturation (were assessed to 18%, Orsi et al., 2002) are added with "±" in the manuscript. Uncertainties in the Pan-Antarctic regions gross and net export fluxes are estimated to be 12.8 and 6.2 Tg C yr^{-1}, respectively.

Text S5

Consistency between three C_{ant} estimating approaches.

The differences between the three approaches could be mostly contained within 10 μmol kg^{-1} (Figs. S6-S7), and a good linear relationship between TrOCA and ΔC* was found at regional scales (Fig. S7). Due to the same assumption on the Redfield ratio (Sabine et al., 2002; Touratier et al., 2007), the C_{ant} obtained by the TTD method based on the CFC-12 associated with ventilation rates and water mass age was more discrete, especially in the deep-water masses of the Ross Sea and Weddell Sea (Fig. S7). The differences between the three methods were largely attributed to the fact that the principal assumptions of the methods don’t fit well to the polar regions well, especially in the estimation of parameters in preformed water masses (Lo Monaco et al., 2005a; Waugh et al., 2006).

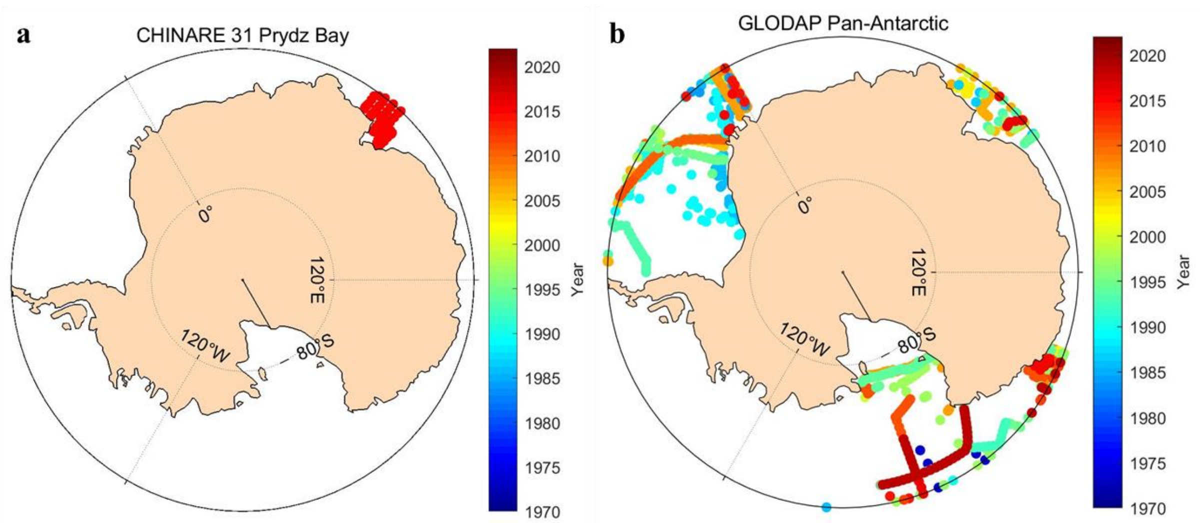

Fig. S1. The distribution of data used in this study, including a, CHINARE31st and GLODAPv2_2022.

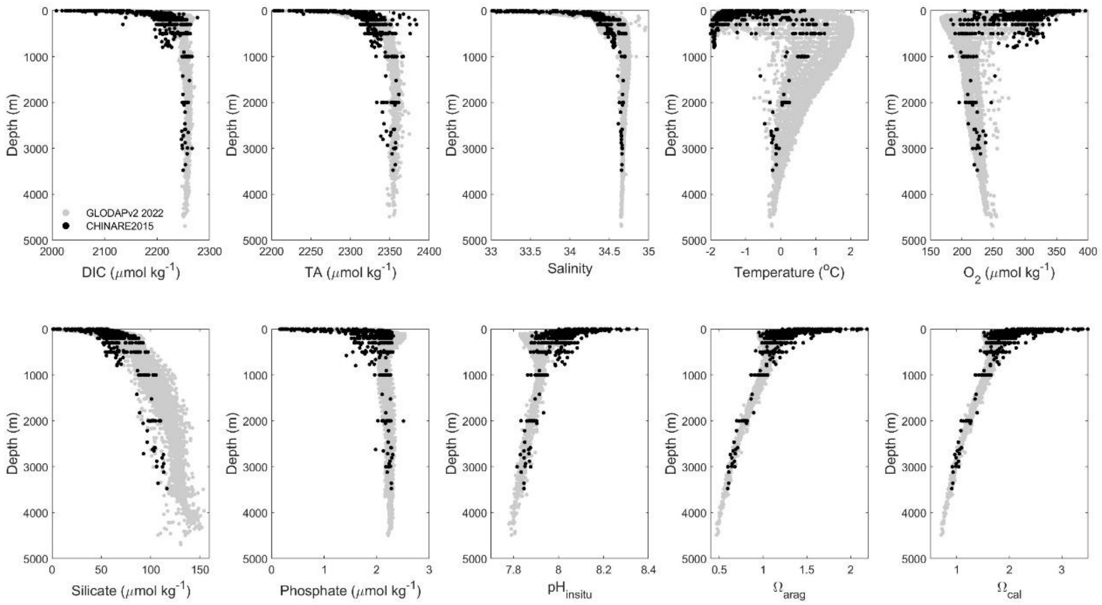

Fig. S2. Comparation of parameters from CHINARE 31st and GLODAP data. The comparation of DIC, TA, Salinity, Temperature, Oxygen, Silicate, Phosphate, pHinsitu, Ω_{arag} and Ω_{cal} in Prydz Bay collected during CHINARE 31st cruise (2015) and the same region in GLODAPv2_2022 (1974-2018) respectively. The grey solid dot is the historical data in GLODAPv2_2022 (1974-2018).

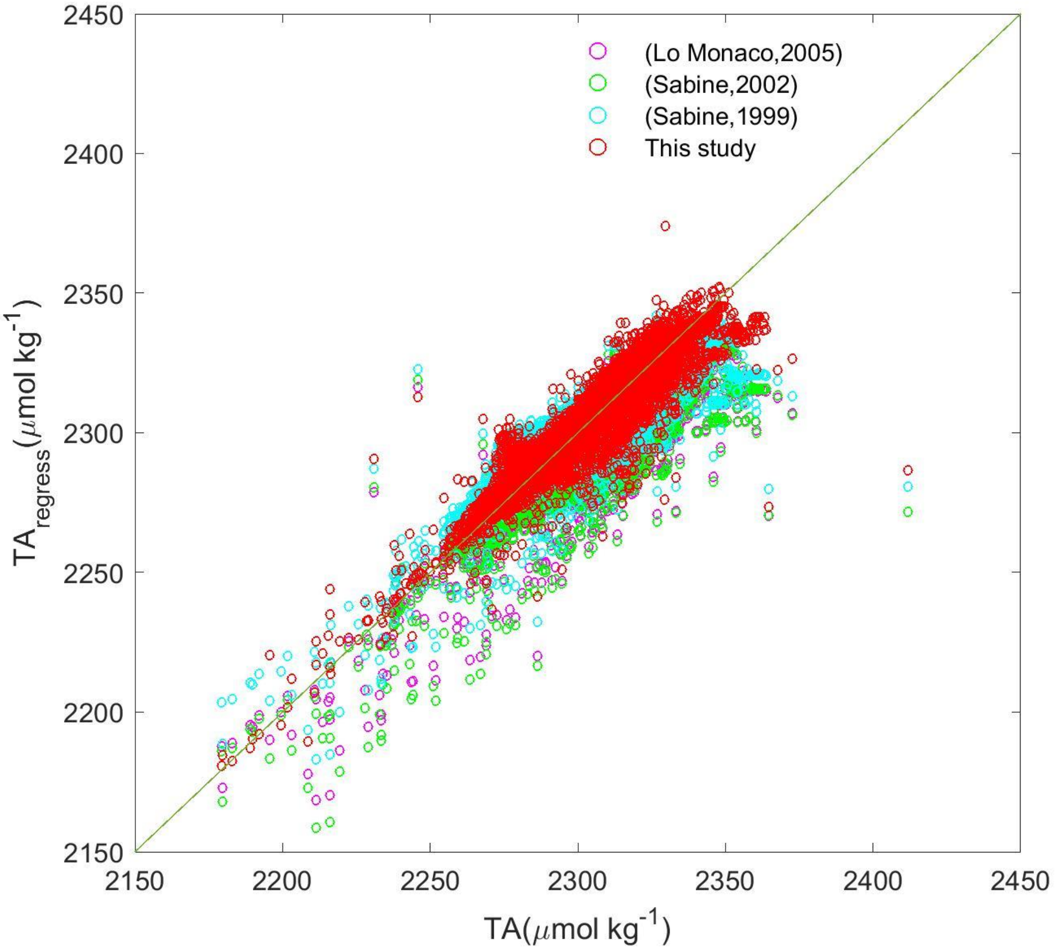

Fig. S3. Comparations of TA^0 regress among this study, Lo Monaco (2005); Sabine (2002); and Sabine (1999). The solid line is 1:1 ratio meaning TAregress = TA.

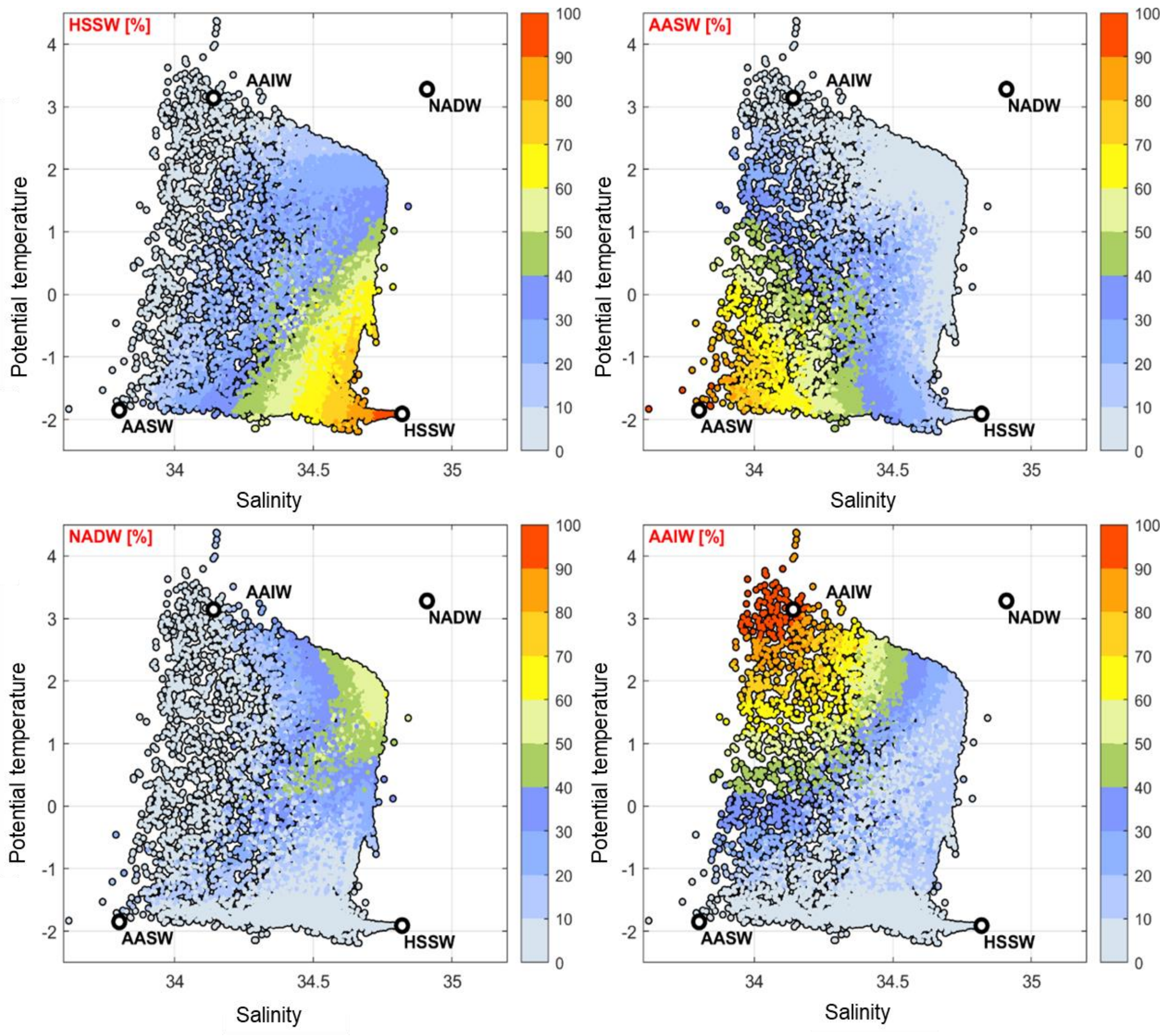

Fig. S4. The results of fractions of different types of water masses by OMP, data based on GLODAP (south of 60°S) and CHINARE 31st.

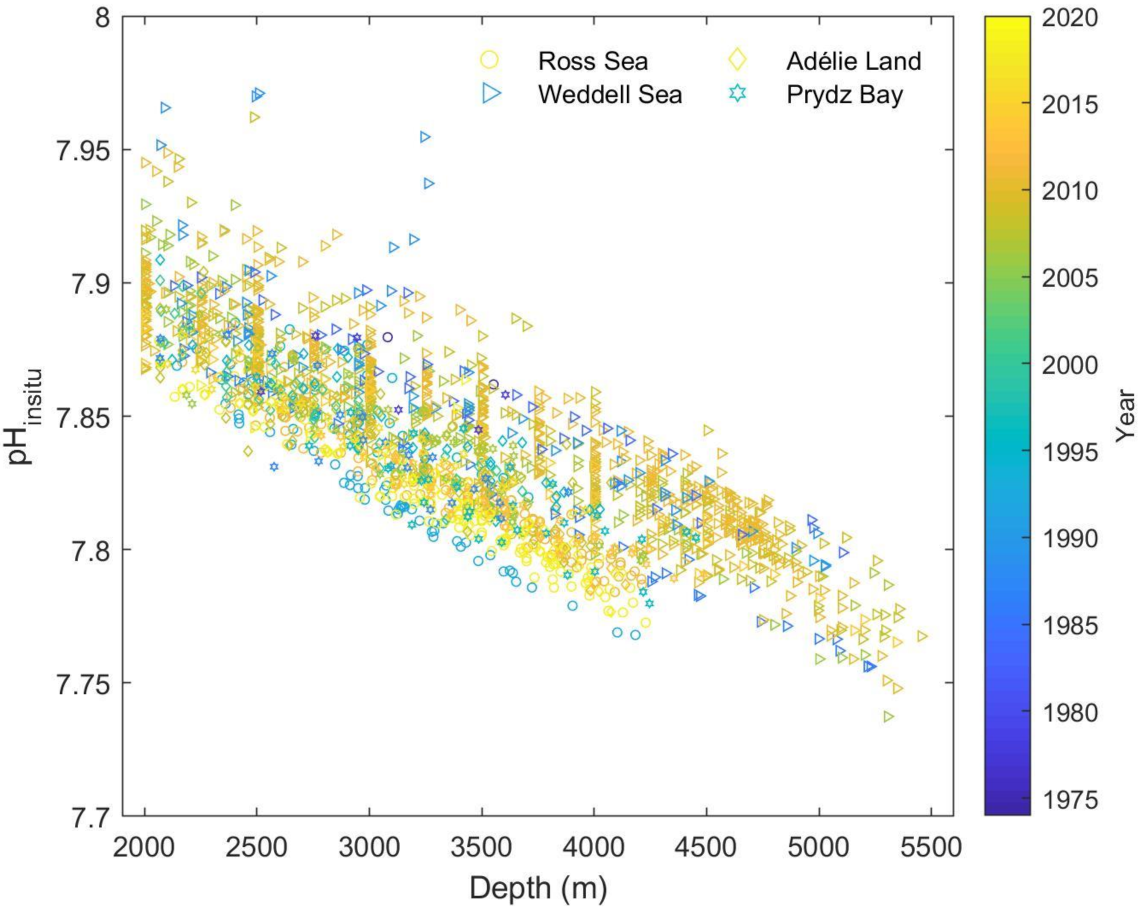

Fig. S5. The relationship between pH_insitu and depth in AABW in four cold shelf regions. pH_insitu is calculated from TA, DIC and nutrients collected from GLODAP v2.2022 and CHINARE 2015 in Fig. S1 and Table S1. AABW are defined in Table S3. The open circle is the Ross Sea, the open right-pointing triangle is the Weddell Sea, the diamond is the Adélie Land, and the hexagram is the Prydz Bay. Color indicates the year of sampling.

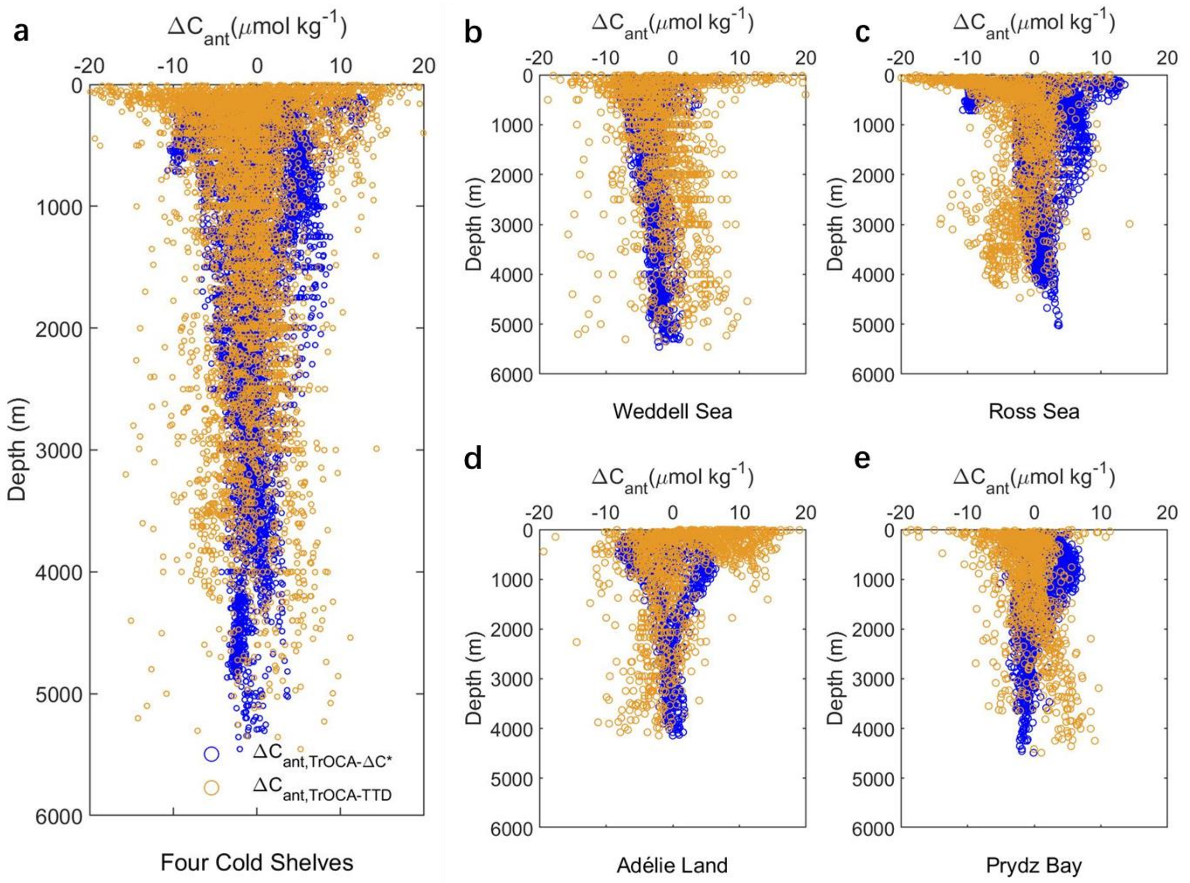

Fig. S6. Distributions of the differences of C_{ant} values from three methods in four cold shelf regions. The ΔC_{ant} calculated from $C_{ant\_TrOCA} - C_{ant\_\Delta C*}$ are marked with blue, and the ΔC_{ant} from $C_{ant\_TrOCA} - C_{ant\_TTD}$ are marked with yellow.

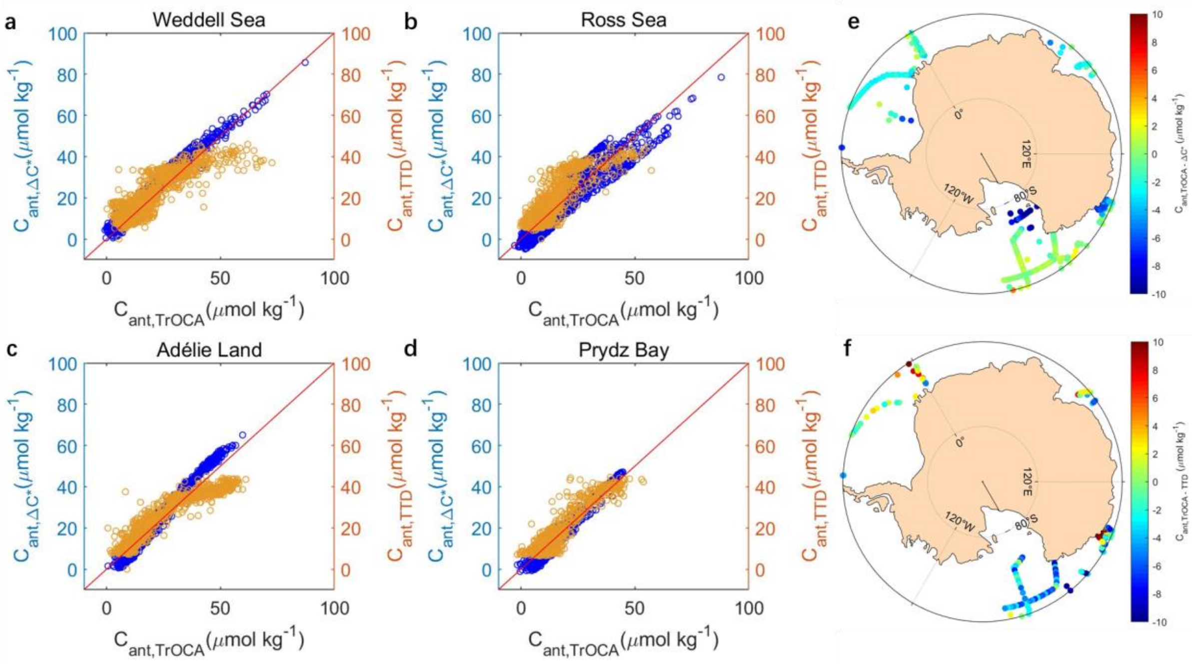

Fig. S7. The relationship between C_{ant} values from three methods (TrOCA, ∆C* and TTD approaches) in the four cold shelves and the distribution of their difference. The differences between ∆C* and TrOCA, TTD and TrOCA are shown in **e** and **f**. The red bold solid lines in **a-d** are 1:1 lines.

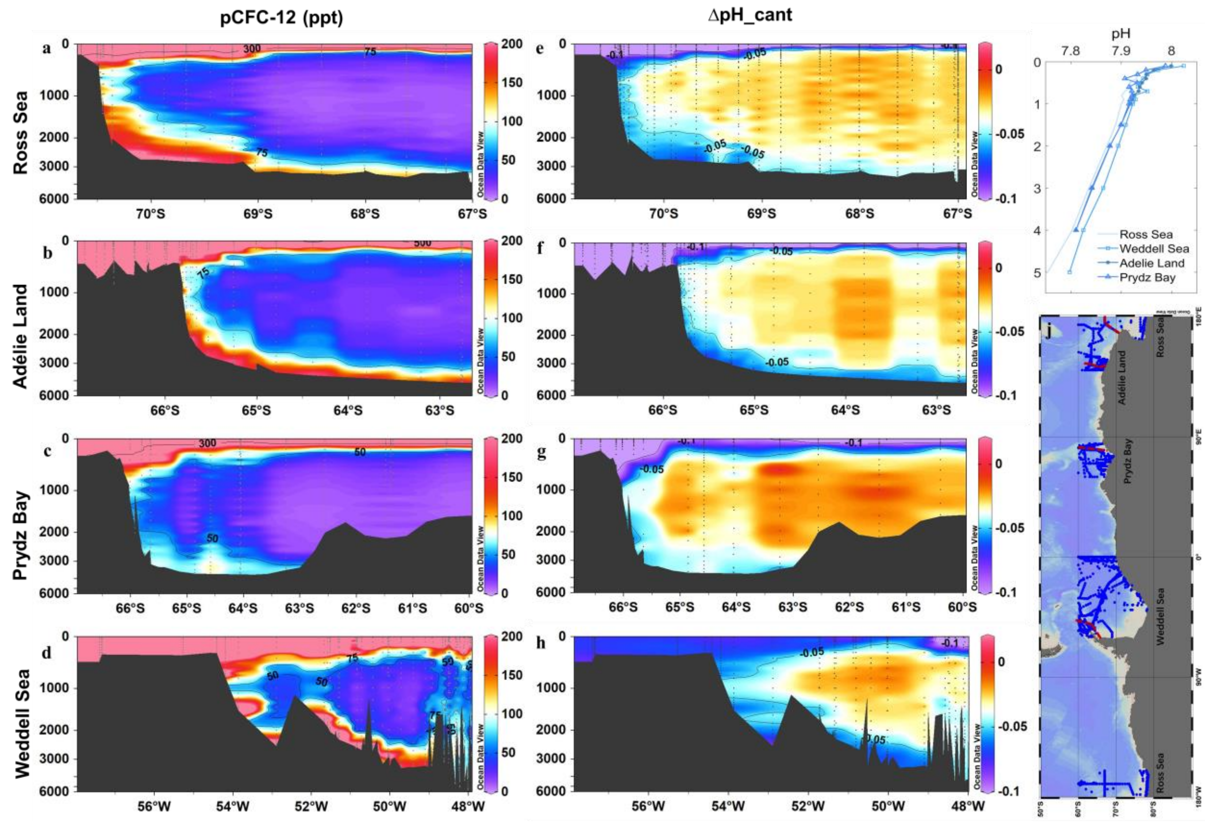

Fig. S8. The vertical distribution of the CFC-12 partial pressure (pCFC-12) and ΔpH_C$_{ant}$ in Four Cold Shelves. ΔpH_C$_{ant}$ is the change in pH due to C$_{ant}$ increase from pre-industrial to 2018. It was calculated from C$_{ant}$ estimated from TrOCA in Methods 2.5 in the Prydz Bay, Weddell Sea, Ross Sea and Adélie Land. Figures drawn by Ocean Data View, Schlitzer, R., Ocean Data View, https://odv.awi.de, 2022. In addition, i is the vertical profile distribution of pH in four cold shelf regions.

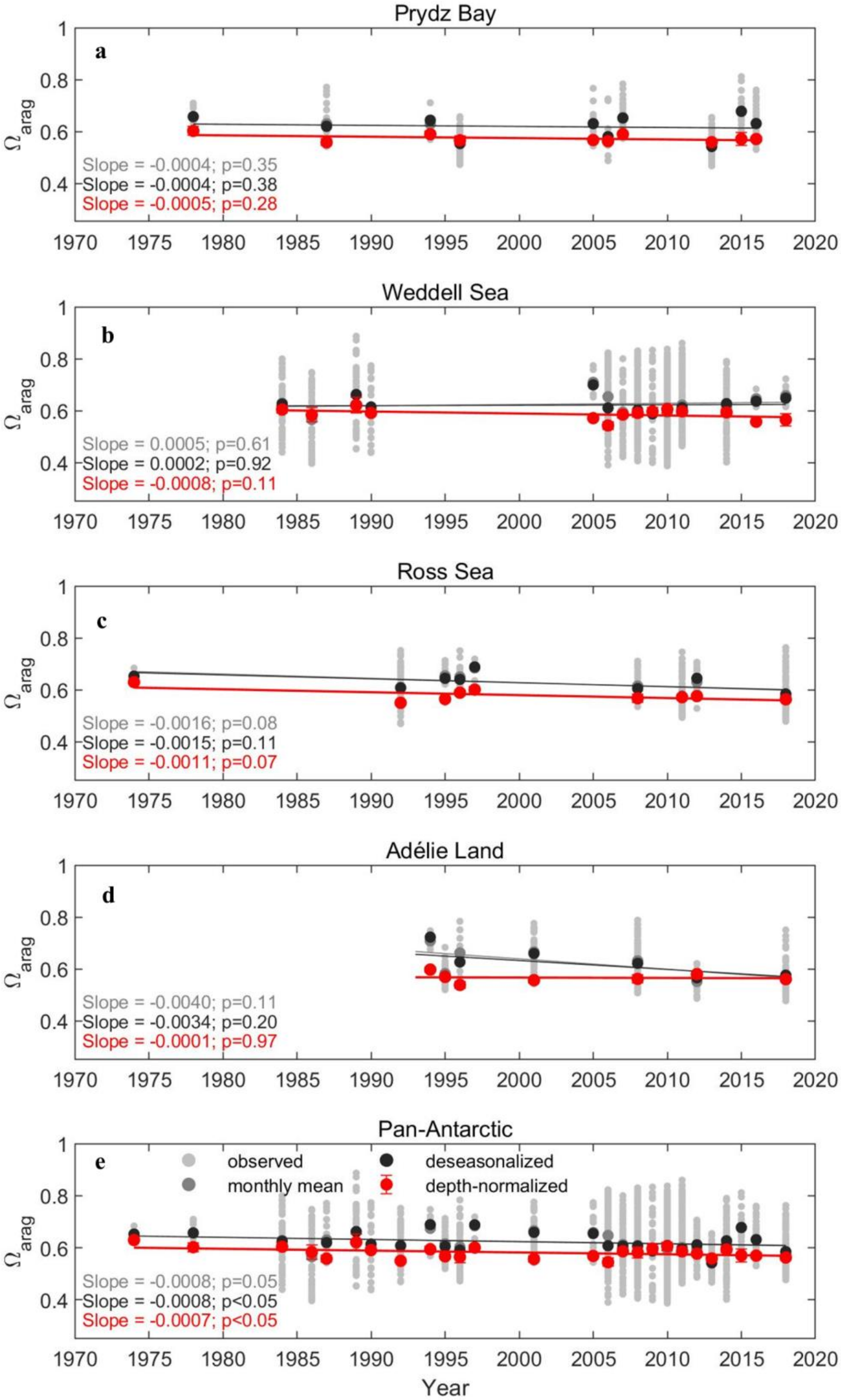

Fig. S9. Long-term trends of Ω_{arag} in the AABW in the Pan-Antarctic shelves. The small grey circle means the observed (or calculated value from observed data), the big grey circle means the monthly mean of observed data, the black and the red circles mean the monthly mean of deseasonalized data and depth-normalized data, respectively (similarly hereinafter).

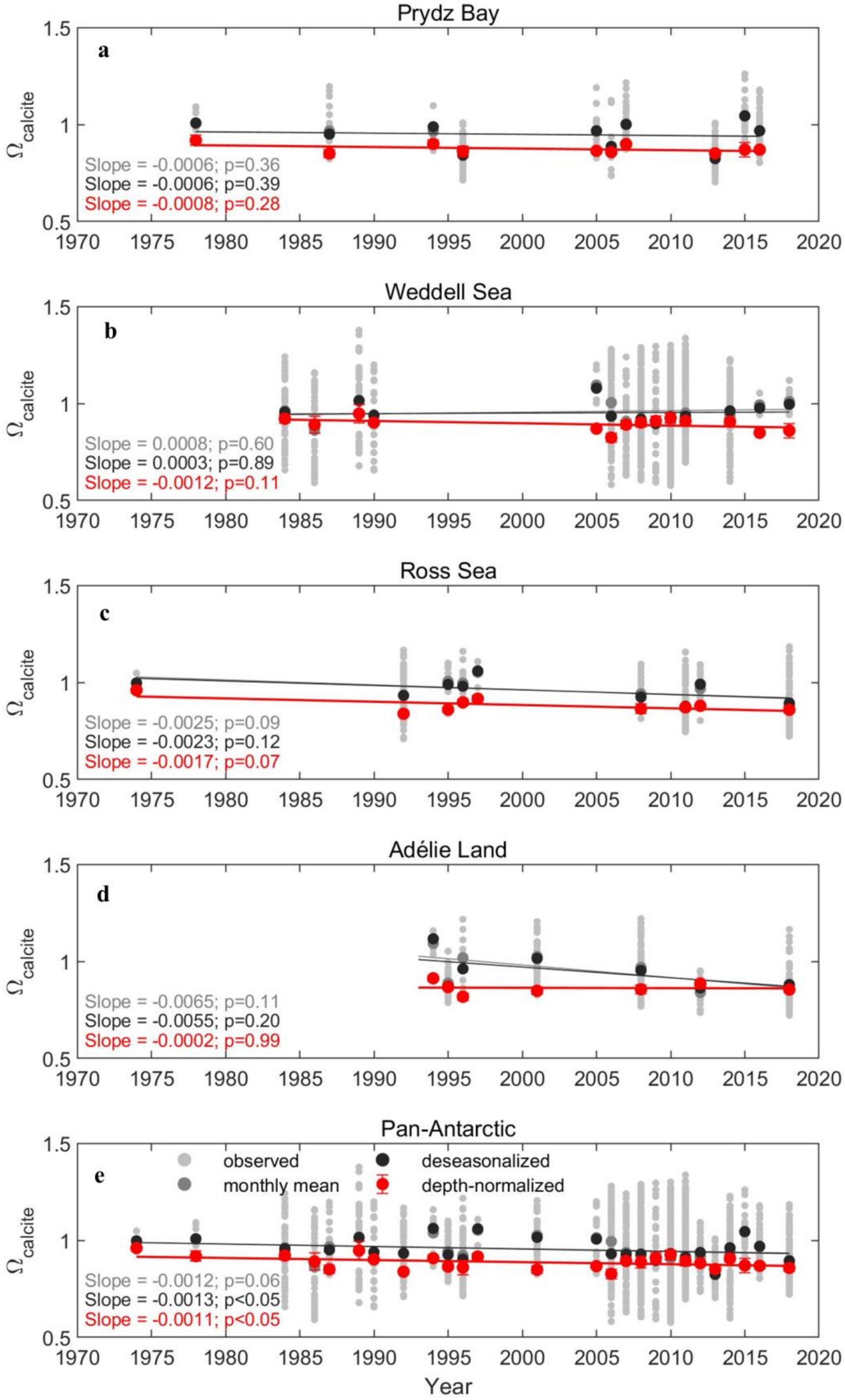

Fig. S10. Long-term trends of $\Omega_{calcite}$ in the AABW in the Pan-Antarctic shelves.

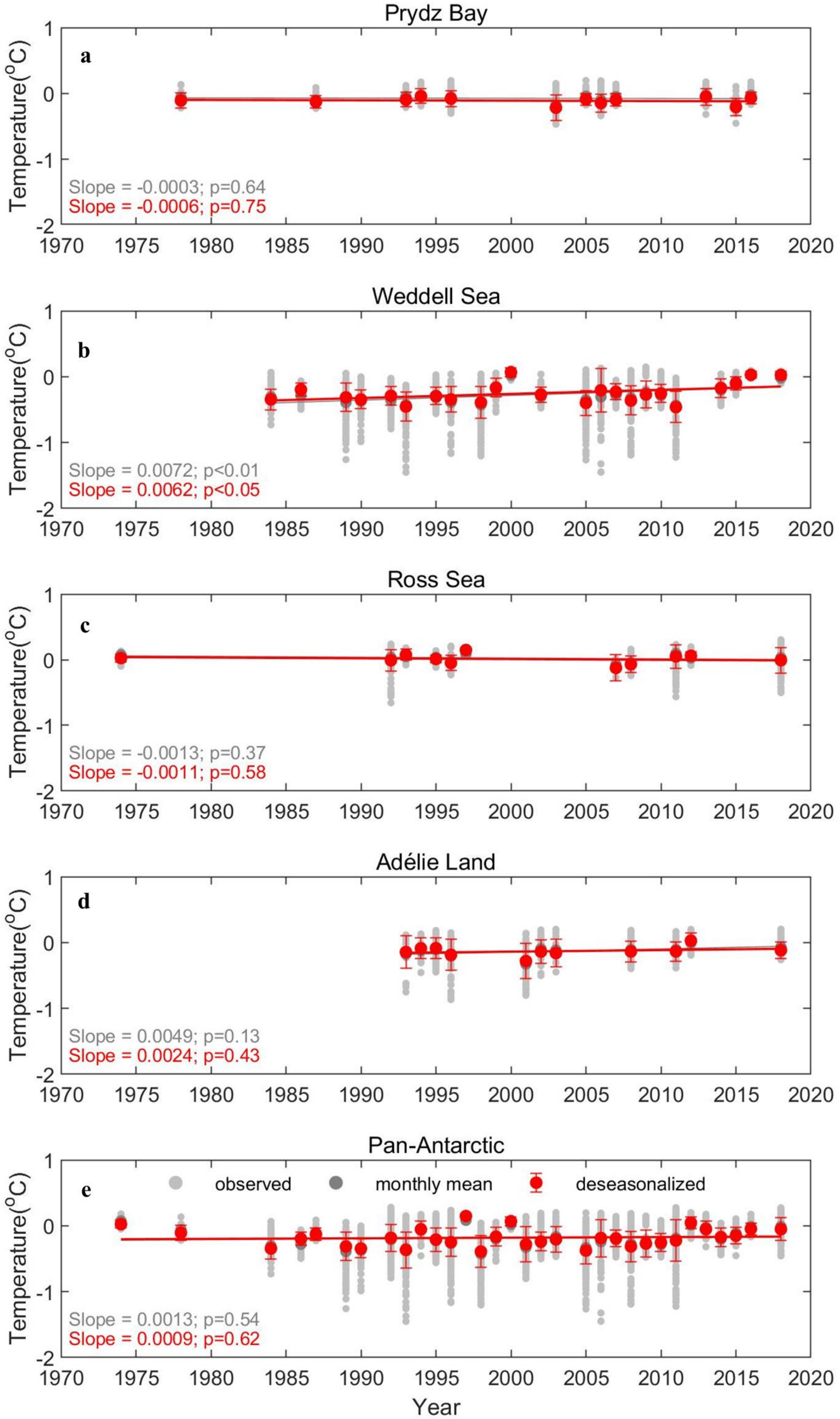

Fig. S11. Long-term trends of temperature in the AABW in the Pan-Antarctic shelves.

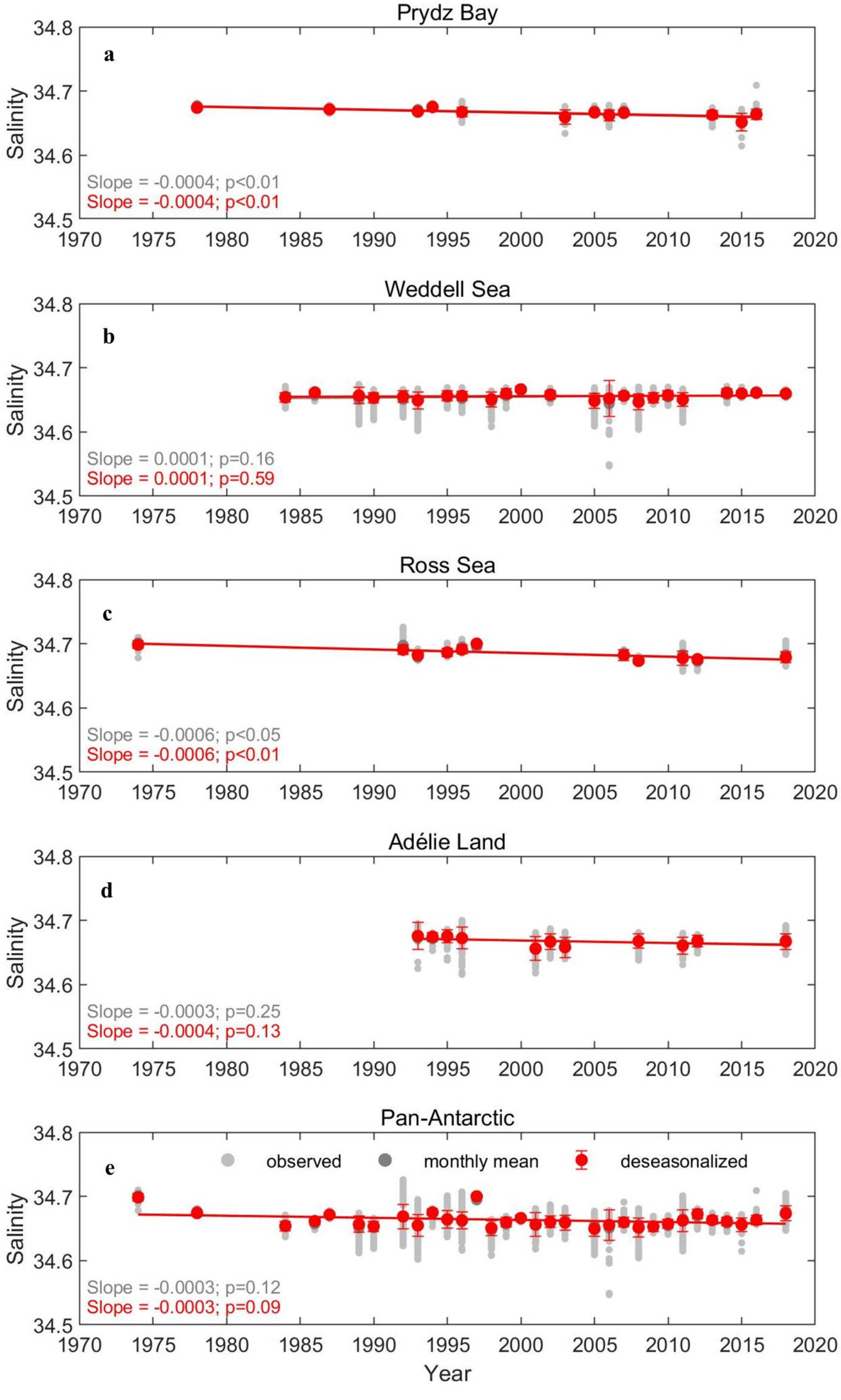

Fig. S12. Long-term trends of salinity in the AABW in the Pan-Antarctic shelves.

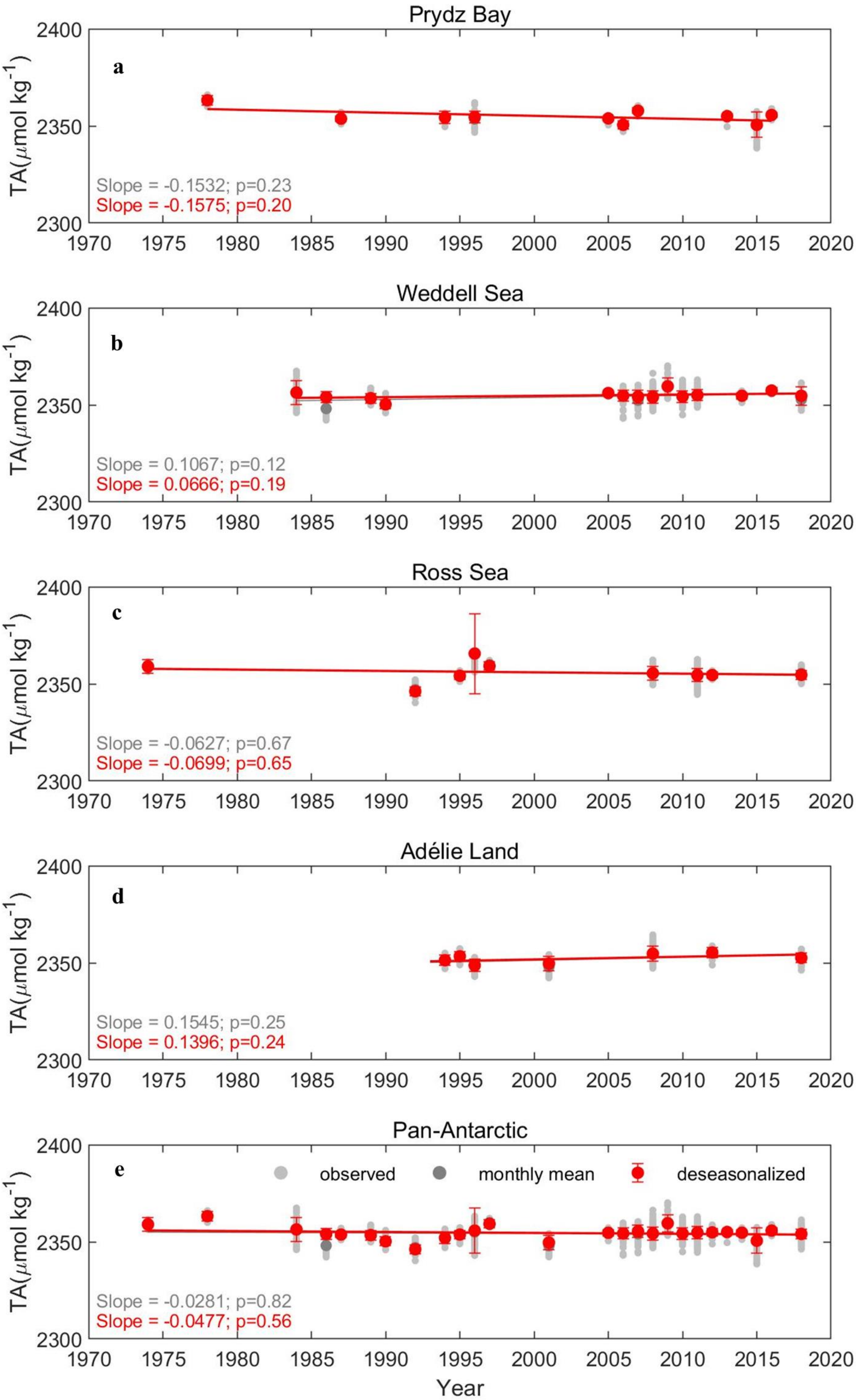

Fig. S13. Long-term trends of TA in the AABW in the Pan-Antarctic shelves.

Table S1. Cruises used for four cold shelf regions.

Regions	Year	Expocode			
Ross Sea	1974	'318M19730822'			
	1992	'90KD19920214'			
	1995	'09AR19941213'			
	1996	'31DS19960105'			
	1997	'320619970113'	'320619970404'	'33RR19971020'	'33RR19971202'
	2008	'09AR20071216'			
	2011	'320620110219'			
	2012	'49NZ20121128'			
	2014	'320620140320'			
	2016	'096U20160426'			
	2018	'096U20180111'	'320620180309'		
Weddell Sea	1984	'316N19831007'			
	1986	'06AQ19860627'			
	1989	'58A119890214'			
	1990	'06MT19900123'			
	2005	'33RO20050111'			
	2006	'06AQ20060825'			
	2007	'06AQ20071128'			
	2008	'06AQ20080210'	'74JC20071231'		
	2009	'740H20081226'	'740H20090203'		
	2010	'06AQ20101128'	'74JC20100319'		
	2011	'06AQ20101128'			
	2014	'06AQ20141202'	'33RO20131223'		
	2016	'74JC20151217'			
	2018	'74JC20181103'			

Table S1 continue

Adélie Land	1994	'09AR19941213'	'49HH19941213'
	1995	'09AR19941213'	
	1996	'09AR19960822'	
	2001	'09AR20011029'	
	2007	'09AR20071216'	
	2008	'09AR20071216'	
	2012	'49NZ20121128'	
	2015	'09AR20141205'	
	2018	'096U20180111'	
Prydz Bay	1978	'318M19771204'	
	1987	'35MF19850224'	
	1994	'316N19941201'	
	1996	'320619960503'	
	2004	'35MF20040103'	
	2005	'09AR20041223'	
	2006	09AR20060102'	
	2007	'33RR20070204'	
	2013	'49NZ20130106'	
	2015	'CHINARE31'	
	2016	'09AR20160111'	'33RR20160208'
	2017	'91AA20171209'	

Table S2. Physical and chemical properties of the water types used in the OMP model to elucidate water mass mixing in the Southern Ocean.

Water type	θ (°C)	Salinity	PO $\mu mol\ kg^{-1}$	NO $\mu mol\ kg^{-1}$	$Si(OH)_4$ $\mu mol\ kg^{-1}$	ΔCdiseq $\mu mol\ kg^{-1}$	Refs.
HSSW	-1.91	34.82	565	565	85	-10	(Pardo et al.,2012)
AASW	-1.85	33.8	617	616	40	-16	(Pardo et al.,2014)
AAIW	3.14	34.14	541	540	15	-8	
NADW	3.28	34.91	430	431	30	-11	
Weights	8	4	3	2	1		(Romera-Castillo et al.,2018)

Table S3. Definitions of the water masses used in this study are listed below. Bounding neutral density (γ_n), salinity, potential temperature (θ), and water depth defining the major water masses in Prydz Bay, Ross Sea, Weddell Sea and Adélie Land are taken from Pardo et al., (2012).

Water Masses	Salinity	θ (°C)	γ_n (kg m^{-3})	Water Depth (m)
AASW	≤34.20	-	≤28.00	<300
DSW	>34.50	<-1.925	>28.27	300~1000
mCDW	>34.50	⩽0.5	28.00~28.27	<1000
CDW	>34.50	>0.5	28.00~28.27	>1000
AABW	>34.60	<0	>28.27	>2000

Table S4. Mean values of partial derivatives for each ocean acidification variable evaluated from the observational dataset.

Partial derivative driver	Ocean acidification variable pH	Ocean acidification variable Ω_{arag}	Ocean acidification variable $\Omega_{calcite}$
$\partial V/\partial T$	-0.0151 ± 0.0003	0.0084 ± 0.0002	0.0124 ± 0.0004
$\partial V/\partial S$	-0.0114 ± 0.0002	-0.0039 ± 0.0005	-0.0076 ± 0.0012
$\partial V/\partial DIC$	-0.0030 ± 0.0000	-0.0038 ± 0.0006	-0.0058 ± 0.0010
$\partial V/\partial TA$	0.0029 ± 0.0000	0.0040 ± 0.0006	0.0061 ± 0.0010

Table S5. Regional air-sea fluxes of CO_2 in the Antarctic coastal seas in the south of 60°S. Fluxes in mmol m^{-2} d^{-1} are multiplied by 120 days to obtain the annual flux mmol m^{-2} yr^{-1}. Based on the previous syntheses, we have further assessed these fluxes by incorporating the most up-to-date flux measurements.

References	Latitude	Year	Subregions	Area ($\times10^6$ km^2)	CO_2 flux (mmol m^{-2} d^{-1})	CO_2 flux (g C m^{-2} yr^{-1})	CO_2 flux (mol C m^{-2} yr^{-1})	Integrated FCO_2 (Tg C yr^{-1})
				Cold Shelf Regions (CSR)				
a	60°−75°S	1993/1996	Weddell Sea	1.70	−1.09 ± 0.95	−4.71 ± 4.12	−0.39 ± 0.34	−8.00 ± 7.00**a**
a	61.4°−75°S	1996	Southern Weddell Gyre	5.00	−2.52**a**	−1.40	−0.12	−7.00**a**
b	55°−75°S	2008−2010	Weddell Sea	6.20	−3.70 ± 2.35	−5.32 ± 3.39	−0.44 ± 0.28	−33.00 ± 21.00**b**
c	55°−67°S	2019	Weddell Sea		−6.90 ± 8.00**c**	−9.94 ± 11.52	−0.83 ± 0.96	−
			Sub-total or average	**0.65**	**−3.55 ± 2.80**	**−**	**−0.45 ± 0.35**	**−3.47 ± 2.75**
d	73-77°S	1994−1996	Ross Sea Polynya	0.33	−10.20**d**	−14.69	−1.22	−4.85
e	76.5°S	1996−1997	Southwestern Ross Sea	0.44	−12.5 ± 8.33	−18.0 ± 12.0	−1.50 ± 1.00**e**	−7.92 ± 5.28
f	73-78°S	1997−2000	Southwestern Ross Sea	−	−7.90 ± 4.20	−11.40± 6.00	−0.95 ± 0.50**f**	−
g	71-78°S	2008	Ross Sea Shelf	−	−15.30	−22.00	−1.84	−13.00**g**
h	65°−80°S	1990−2011	Ross Sea	0.47	−7.67 ± 3.67	−11.0 ± 5.28	−0.92 ± 0.44**h**	−5.19± 2.48
h	71°−79°S	2003−2013	Ross Sea		−10.83 ± 0.83	−15.6 ± 1.20	−1.30 ± 0.10**h**	−7.50 ± 0.50**h**
			Sub-total or average	**0.59**	**−10.74 ± 2.51**	**−**	**−1.29 ± 0.30**	**−9.12 ± 2.13**
i	64°−68°S	1994/95	Adélie Land	−	−2.30 ± 2.25**i**	−3.31 ± 3.24	−0.28 ± 0.27	−
j	64°−68°S	1999,2001,2008,2011	Adélie Land	0.08	−35.0 ± 20.0**j**	−25.20 ± 14.40	−2.10 ± 1.20	−2.02 ± 1.15
k	65.5°−68.5°S	2015,2017	Adélie Land	−	−6.56 ± 4.33**k**	−9.45 ± 6.24	−0.79 ± 0.52	−
			Sub-total or average	**0.16**	**−14.62 ± 6.86**	**−**	**−1.05 ± 0.45**	**−2.02 ± 0.85**
l	68.6°S	1993−1995	Prydz Bay	−	−32.80**l**	−26.40	−2.20**l**	−
m	58−65°S	2000	Indian Antarctic sector	−	−3.00 ± 1.41**m**	−4.32 ± 2.03	−0.36 ± 0.17	−
n	60−70°S	1999/2000	Prydz Bay	−	−2.50**n**	−3.60	−0.30	−
o	68.5°−68.6°S	2010−2011	Prydz Bay	−	−6.56 ± 4.33**o**	−9.54 ± 6.24	−0.79 ± 0.52	−
o	60−70°S	2006	Prydz Bay	−	−8.00 ± 21.0**o**	−5.76 ± 15.12	−0.48 ± 1.26**o**	−

Table S5 continued

p	60°−72°S	2009−2012	Enderby Basin	–	−28.4 ± 45.6**p**	−40.9 ± 65.7	−3.41 ± 5.47	–
q	66°−67°S	2014/2015	Dalton Polynya	–	0.70 ± 0.90**q**	1.00 ± 1.30	0.08 ± 0.11	–
r	64°−70°S	2015	Prydz Bay	–	−24.55 ± 6.57**r**	−35.4 ± 9.50	−2.95 ± 0.79	–
s	66°−68°S	2009	Cape Darnley Polynya	–	−6.50 ± 6.90**s**	−9.36 ± 9.94	−0.78 ± 0.83	–
t	64°−70°S	2015	Prydz Bay	–	−21.40 ± 27.30**t**	−30.8 ± 39.3	−2.57 ± 3.28	–
			Sub-total or average	**0.14**	**−13.30 ± 7.27**	**–**	**−2.30 ± 1.61**	**−2.31 ± 1.39**
			Sub-total of CSR	**1.54**	**–**	**–**	−**1.04 ± 0.26**	−**16.93 ± 3.84**
	60°-80°				***Non-Cold Shelf Regions (NCSR)***			
u	68°−75°S	2009.1−2	Amundsen Sea	0.05	−15.90 ± 13.80**u**	−22.90 ± 19.90	−1.91 ± 1.66	−1.14 ± 0.99
u	71°−73.7°S	2010−2011	Amundsen Sea Polynya	0.03	−18.0 ± 14.0**u**	−25.9 ± 20.2	−2.16 ± 1.68	−0.78 ± 0.60
			Sub-total or average	**0.25**	**−16.95 ± 9.83**	**–**	**−2.03 ± 1.18**	**−6.10 ± 3.54**
v	62°−65.5°S	1995−1996	Bellingshausen Sea		−7.55 ± 6.62v	−10.9 ± 9.53	−0.91 ± 0.79	−3.37 ± 2.96
			Sub-total or average	**0.31**	**−7.55 ± 6.62**	**–**	**−0.91 ± 0.79**	**−3.37 ± 2.96**
w	67.5°−67.7°S	2011−2013	WAP (Ryder Bay)	–	−7.50 ± 4.58	−10.80 ± 6.60	−0.90 ± 0.55**w**	–
w	60°−65°S	2008−2010	NAP	–	−1.07 ± 1.30**w**	−4.62 ± 5.62	−0.39 ± 0.47	–
w	62°−65°S	2016	NAP	–	−25.30 ± 8.48**w**	−36.40 ± 12.20	−3.04 ± 1.02	–
w	63.5°−65°S	2002−2017	NAP	–	1.24 ± 4.33**w**	−1.79 ± 6.24	−0.15 ± 0.52	–
w	63.5°−65°S	1999−2017	NAP	–	−12.00 ± 13.00**w**	−17.28 ± 18.72	−1.44 ± 1.56	–
w	63.5°−65°S	2015	NAP	–	0.50 ± 0.45**w**	0.72 ± 0.65	0.06 ± 0.05	–
w	62°−63°S	2013	Gerlache Strait	–	−0.07**w**	−0.10	−0.01	–
			Sub-total or average	**0.29**	**−4.17 ± 2.80**	**–**	**−0.54 ± 0.34**	**−1.87 ± 1.20**
p	60°−69°S	2009−2012	**Western Indian Sector**	**0.30**	**−6.35 ± 0.64p**	**–**	**−0.76 ± 0.08**	**−2.74 ± 0.28**
o	60°−70°S	2018/2019	**Eastern Indian Sector**	**0.16**	**0.58 ± 1.08**	**–**	**0.07 ± 0.13o**	**0.13 ± 0.25**
			Sub-total of NCSR	**1.31**	−**6.89 ± 2.45**	**–**	−**0.83 ± 0.29**	−**13.95 ± 4.78**

Table S5 continued

				Antarctic Shelves & coastal seas in Southern Ocean				
This study			**Total Pan-Antarctic**	**2.85**	**−8.70 ± 1.81**	–	**−0.90 ± 0.20**	**−30.88 ± 6.13**
BG, 2016	65°−80°S	1993−2012	Antarctic Shelves	2.45	–	–	−0.90±0.15	−26.63±3.99
LA,2014	65°−80°S	1990−2011	Antarctic Shelves	2.95	–	–	−0.14	−5.38
RO,2019	65°−80°S >45°S	1998−2015	Coastal seas in SO	2.69	–	–	−0.12±0.10	−3.80±2.55 −17.0±3.00(45°S)
DA,2022	60°−75°S	2000 –2020	Antarctic Shelves	2.95	–	–	−0.53±0.32	−18.80±11.30

Note: North Antarctic Peninsula (NAP); West Antarctic Peninsula (WAP); Western Antarctic Shelves (WAS); Eastern Antarctic Shelves (EAS); Southern Ocean (SO).

a. *Hoppema et al.* (1999) reported an annual CO_2 uptake of −8.00 ± 7.00 Tg C yr^{-1} (−0.39 ± 0.34 mol C m^{-2} yr^{-1}) for the offshore western Weddell Sea by the budget of upper-layer based on cruises during the period of April/May 1996 and December/January 1993 and a surface area of the 1.70×10^6 km^2. *Hoppema et al.*, (2000) reported a net CO_2 uptake is −2.52 mmol C m^{-2} d^{-1} of the entire Weddell Gyre region based on the earlier cruises and previous studies, and obtained a total flux of 7.00 Tg C yr^{-1} within a 45-day duration and an area of 5×10^6 km^2.

b. *Brown et al.* (2015) reported the annual mean fluxes of −33.0 ± 21.0 Tg C yr^{-1} based on the surface layer balance budget, and −12.0 ± 24.0 Tg C yr^{-1} derived from the neutral network sea surface for the period of 2008−2010, with an area of 6.20×10^6 km^2.

c. *Ogundare et al.* (2019) reported a flux of −6.90 ± 8.00 mmol C m^{-2} d^{-1} for the autumn in the Weddell Gyre region estimated from direct observations between February and April 2019.

d. *Bates et al.* (1998) reported a value of −10.20 mmol CO_2 m^{-2} d^{-1} for the ice-free period of 4 months (from mid-December to mid-February each year) based on two cruises to the Ross Sea polynya in November/December 1994 and December 1995 to January 1996. The open area was ~0.33×10^6 km^2.

e. *Sweeney* (2003) calculated an annual air-sea flux of −1.5 ± 1.0 mol C m^{-2} yr^{-1} from the surface data during 1996 and 1997, considering sea ice concentrations around 76.5°S between 170°W and 182°W in the southwestern Ross Sea.

f. *Arrigo and van Dijken* (2007) reported annual CO_2 fluxes between 1986 and 1994 ranging from −0.1 to −0.57 mol C m^{-2} yr^{-1}. Also a spatial annual flux of −1.45 mol C m^{-2} yr^{-1} for the southwestern Ross Sea during normal ice years (from 1998−1999, 1999−2000 and 2001−2002) and −0.45 mol C m^{-2} yr^{-1} during three heavy ice years (1997−1998 and 2000−2001, 2002−2003) based on the Coupled Ice, Atmosphere, and Ocean (CIAO) model, gives an annual flux of −0.95 ± 0.5 mol C m^{-2} yr^{-1} from 1997−2003 in this southwestern Ross Sea.

g. *Arrigo et al.* (2008) reported a total atmospheric CO_2 sink on the Ross Sea continental shelf of 13 TgC yr^{-1} based on the Coupled Ice, Atmosphere, and Ocean (CIAO) model.

h. *DeJong and Dunbar* (2017) calculated CO_2 flux rates with in situ and wind speed data from 20 cruises in the Ross Sea region (160°E–155°W, 71°S–79°S) and found that the Ross Sea was an atmospheric CO_2 sink with −1.30 ± 0.1 mol C m^{-2} yr^{-1} (−7.5 ± 0.5 Tg C yr^{-1}) from 2004 to 2013, assuming negligible CO_2 flux between April and October. *Laruelle et al.* (2014) also reported a more moderate atmospheric CO_2 sink of –0.92 ± 0.44 mol C m^{-2} yr^{-1} over the period of 1990−2011.

i. *Ishii et al.* (2002) calculated the air-sea CO_2 flux of the Seasonal Ice Zone (SIZ, the south of 64°S around 140°E) during a cruise in the austral summer of 1994/95, from −3.50 ± 2.80 mmol C m^{-2} d^{-1} in December to −1.10 ± 1.70 mmol C m^{-2} d^{-1} in January. We take a mean flux of −2.30 ± 2.25 mmol C m^{-2} d^{-1} for the summer time.

j. *Shadwick et al.* (2013, 2014) reported a CO_2 flux of −15.00 mmol C m^{-2} d^{-1} in summer 2007/2008 and −30.00~−80.00 mmol C m^{-2} d^{-1} in 2011 based on four voyages (one winter voyage in 1999 and summer voyages in 2001, 2008 and 2011) to the Mertz Polynya regions . We used the mean flux of −35.0 ± 20.0 mmol C m^{-2} d^{-1} for summer time. The surface area of the ice-free region is 0.08×10^6 km^2.

k. *Arroyo et al.* (2020) reported an average flux of approximately −6.56 ± 4.33 mmol C m^{-2} d^{-1} over the Jan. 2015 and Jan. 2017 cruises.

l. *Gibson and Trull* (1999) reported an air-sea CO_2 flux of −32.8 mmol m^{-2} d^{-1} and an annual flux of −2.2 mol C m^{-2} yr^{-1} during the summer ice-free period (1993−1995).

m. *Metzl et al.* (2006) reported an oceanic CO_2 sink of −2 to −4 mmol m^{-2} d^{-1} in the seasonal ice zone (south of 58°S) in the austral summer based on observations obtained in January and August 2000 during OISO cruises in the Indian Antarctic sector. Here we take a mean flux of −3.00 ± 1.41 mmol m^{-2} d^{-1}.

n. *Gao et al.* (2008) reported a flux of Prydz Bay (60−70°S) −2.50 mmol m^{-2} d^{-1} in January during cruises from November 1999 to April 2000.

o. *Roden et al.* (2013) estimated an annual air-sea CO_2 flux of −6.56 ± 4.33 mmol C m^{-2} d^{-1} in Prydz Bay during May 2010 to Feb. 2011. The mean air-sea CO_2 flux of −8.00 ± 21.0 mmol m^{-2} d^{-1} and −0.48 mol C m^{-2} d^{-1} in the seasonal ice zone off the coast of East Antarctica and a weak source of 0.07 ± 0.13 mol C m^{-2} yr^{-1} in ice free days were reported by *Roden et al.* (2016), whose observations were made during the austral summer (Jan. to Mar. 2006) at 30−80°E.

p. *Shetye et al.* (2017) reported that in the Enderby Basin (20°−70°E), located in the Antarctic coastal region, Indian sector, the average of air-sea CO_2 flux is −28.4 ± 45.6 mmol C m^{-2} d^{-1} from 2009 to 2012 (Mar. 2009, Feb. 2010, Jan. 2012). Along west of 55°E, the CO_2 fluxes averaged −6.8 mmol m^{-2} d^{-1} and −5.9 mmol C m^{-2} d^{-1} during February and March, here we take the mean value of −6.35 ± 0.64 mmol C m^{-2} d^{-1} as the air-sea CO_2 flux of the western Indian Sector.

q. *Arroyo et al.* (2018) reported that the Dalton Polynya was a net source of CO_2 to the atmosphere, 0.70 ± 0.90 mmol C m^{-2} d^{-1}, during the summer of 2014/2015 using high-frequency underway measurements of CO_2 fugacity.

r. *Xu et al.* (2019) reported that Prydz Bay was mainly a strong CO_2 sink in February 2015, with a flux of −23.57 ± 6.36 Tg C $month^{-1}$ (−24.55 ± 6.57 mmol C m^{-2} day^{-1}) using a neural network technique based on in situ averages obtained during the 31st CHINARE cruise from February to early March 2015.

s. *Murakami et al.* (2020) reported the mean air-sea CO_2 flux of −6.50 ± 6.90 mmol m^{-2} d^{-1} in the Cape Darnley polynya, East Antarctica (66–68°S, 67–71°E) from 22 to 27 January 2009.

t. *Wang et al.* (2020) reported a mean CO_2 flux is −21.40 ± 27.3 mmol m^{-2} d^{-1} during Feb. 2015. The ice-free period is three months per year with an area of 0.08×10^6 km^2.

u. *Tortell et al.* (2012) reported an overall mean air-sea CO_2 flux of −15.9 ± 13.8 mmol C m^{-2} d^{-1} (11 Jan to 16 Feb 2009). The mean polynya size was 5.00×10^4 km^2, and the open water of the AP and PIP was present for ~145 days in 2008−2009. *Mu et al.* (2014) reported an overall mean air-sea CO_2 flux of the Amundsen Sea Polynya, −18.0 ± 14.0 mmol C m^{-2} d^{-1}, during the austral summer of 2010−2011. The mean open water area of the ASP from 1997−2010 was 27.3×10^3 km^2.

v. *Álvarez et al.* (2002) reported a mean CO_2 flux of the Bellingshausen Sea of −6.5 ± 6 and −4 ± 2.6 mmol m^{-2} d^{-1}, and a mean CO_2 flux of the Gerlache Strait of −3.8 ± 4.2 and −15.9 ± 13.7 mmol m^{-2} d^{-1} during austral summer of 1995−96.

Legge et al. (2015) reported a net sink of atmospheric CO_2 of −0.56~−1.34 mol C m^{-2} yr^{-1} (average of 3 years, 2011−2013). Here we use the average value of −0.90 ± 0.55 mol C m^{-2} yr^{-1}, assuming that the mean daily open water area of the Ryder Bay, west Antarctic Peninsula (WAP) is 1.20×10^2 km^2. *Ito et al.* (2018) reported the CO_2 flux of −1.00, 0.20, −2.40 mmol CO_2 m^{-2} d^{-1} in the northern Antarctic Peninsula (including Bransfield, Weddell Sea, Drake Passage) during three summer periods (2008-2010), here we take the average of three years as the mean flux −1.07 ± 1.30 mmol CO_2 m^{-2} d^{-1}, based on the 0.32×10^6 km^2 in the summers of 2008−2010. *Costa et al.* (2020) reported a mean flux of −25.8 ± 8.48 mmol C m^{-2} d^{-1} in the Northern Antarctic Peninsula (NAP) during a late summer study in February 2016. *Monteiro et al.* (2020a) reported an annual net sea-air CO_2 flux of 1.24 ± 4.33 mmol m^{-2} day^{-1} from 2002−2017 in the northern Antarctic Peninsula based on Surface Ocean CO_2 Atlas version 6 (SOCATv6). *Monteiro et al.* (2020b) reported that Gerlache Strait was on average an atmospheric CO_2 sink –12 ± 13 mmol m^{-2} d^{-1} during austral summers (Jan. – Mar.) from 1999 to 2017 based on a compiled dataset. *Kerr et al.* (2018) reported that the Gerlache Strait was a carbon source with an average flux of 0.50 ± 0.45 mmol m^{-2} d^{-1} during February 2015. *Caetano et al.* (2020) also reported a nearly neutral air-sea CO_2 flux with a value of −0.07 mmol m^{-2} d^{-1} in Dec. 2013 based on high-resolution data in Admiralty Bay in the northern Antarctic Peninsula.

w. *Tozawa et al.* (2021) report a mean CO_2 flux of −8.30 ± 12.7 mmol m^{-2} d^{-1} during Dec. 2018 to Jan. 2019 in the seasonal ice zone of the Eastern Indian Sector (south of 60°S).

x. Based on BG (2016) (Bourgeois et al., 2016), LA (2014) (Laruelle et al., 2014), RO (2019) (Roobaert et al., 2019), DA (2022) (Dai et al., 2022).

Table S6. Estimated contributions to the long-term Ω_{arag} ($\Omega_{calcite}$) saturation trends in AABW of Pan-Antarctic from 1974-2018.

	Driver	Driver rate of change (yr^{-1})	Changes in drivers (1974~2018)	Contribution to the long-term trends Ω (units yr^{-1})
Thermal component	ΔT	0.001 ± 0.001℃	0.04 ± 0.05 ℃	0.00001 ± 0.00001 (0.00001 ± 0.00001)
Non-thermal Component	ΔsDIC	0.15 ± 0.04 μmol kg^{-1}*	6.73 ± 1.59 μmol kg^{-1}	−0.0006 ± 0.0002 (−0.0009 ± 0.0003)
	ΔsDIC_C_{ant}♯	0.14 ± 0.03 μmol kg^{-1}**	6.09 ± 1.20 μmol kg^{-1}	−0.0005 ± 0.0001 (−0.0008 ± 0.0002)
	ΔsDIC_C_{nat}♯	0.01 ± 0.05 μmol kg^{-1}	0.64 ± 1.99 μmol kg^{-1}	−0.0001 ± 0.0002 (−0.0001 ± 0.0003)
	ΔsTA	−0.05 ± 0.03 μmol kg^{-1}	−2.10 ± 1.36 μmol kg^{-1}	−0.0002± 0.0001 (−0.0003 ± 0.0002)
	ΔS(freshwater)	−0.0003 ± 0.0001 ppt	−0.013 ± 0.003 ppt†	−0.000006 ± 0.000002 (−0.000009 ± 0.000002)
Sum			−0.03 ± 0.01 (−0.05 ± 0.02)	−0.0008 ± 0.0003 (−0.0012 ± 0.0005)
Observed			−0.03 ± 0.00 (−0.05 ± 0.01)	−0.0007 ± 0.0001 (−0.0011 ± 0.0002)
C_{ant} pre-industrial-2018			−0.06 ± 0.02 (−0.09 ± 0.03)	

The thermal and non-thermal components were separated by normalizing the pH to S=34.66 (the mean salinity value of the AABW in four regions). Rates (± standard error of slope) were estimated by linear regression using annual means. Asterisks indicate the levels of significance of the trends (**P < 0.01, *P < 0.05).

†Parts per thousand (ppt) measures the salinity of seawater.

♯The ΔDIC_C_{ant} and ΔDIC_C_{nat} indicate the changes in DIC due to anthropogenic CO_2 (TrOCA-based) and natural CO_2.